

# Nonclassical Longitudinal Magnetoresistance in Anisotropic Black Phosphorus

Francesca Telesio,\* Nicholas Hemsworth, William Dickerson, Matei Petrescu, Vahid Tayari, Oulin Yu, David Graf, Manuel Serrano-Ruiz, Maria Caporali, Maurizio Peruzzini, Matteo Carrega, Thomas Szkopek, Stefan Heun, and Guillaume Gervais

Resistivity measurements of a black phosphorus (bP) field-effect transistor 16 nm thick in parallel magnetic fields up to 45 T are reported as a function of the angle between the in-plane field and the source–drain (S–D) axis of the device. The crystallographic directions of the bP crystal are determined by Raman spectroscopy, with the zigzag axis found to be within 5° of the S–D axis and the armchair axis in the orthogonal planar direction. A transverse magnetoresistance (TMR) as well as a classically forbidden longitudinal magnetoresistance (LMR) are observed. Both are found to be strongly anisotropic and nonmonotonic with increasing in-plane field. Surprisingly, the relative magnitude (in %) of the positive LMR is larger than the TMR above ≈32 T. Considering the known anisotropy of bP whose zigzag and armchair effective masses differ by a factor of ≈7, the experiment strongly suggests this LMR to be a consequence of the anisotropic Fermi surface of bP.

Magnetoresistance (MR) is a phenomenon in which a material's resistivity increases or decreases due to the presence of a magnetic field  $\mathbf{B}$ . Transport measurements typically require the presence of an electric field  $\mathbf{E}$  so as to establish an average

current with charge velocity  $\mathbf{v}$  along a preferred direction. The overall force on the charge carriers  $q$  (electrons or holes) is simply given by Lorentz force,  $\mathbf{F} = q(\mathbf{E} + \mathbf{v} \times \mathbf{B})$ . From this stems two important limiting cases: one where the current flow is perpendicular to  $\mathbf{B}$  and for which the magnitude contribution of the Lorentz force is maximal and the other where it is parallel to  $\mathbf{B}$ , and there is no magnetic contribution to Lorentz force. This simple classical picture, therefore, implies that MR is forbidden in the latter case. However, decades of research has shown that a material can develop a longitudinal magnetoresistance (LMR) when the current and the magnetic field are parallel. The exact set of conditions for which a nonclassical LMR can or cannot

be observed remains a highly debated topic which has gained renewed interest recently within the context of Weyl semimetals and topological insulators.<sup>[1–3]</sup>

Pal and Maslov<sup>[4]</sup> have studied theoretically nonclassical LMR on generic grounds. They proposed a set of necessary and sufficient conditions within the context of Fermi surface (FS) morphology for a 3D system. While not all anisotropy lead to LMR, it was shown that an angular anisotropy of the FS along the magnetic field direction is a sufficient condition. Black phosphorus (bP) provides a key system for this as its FS is highly anisotropic with effective masses for holes,  $m_{ac} = 0.11m_0$  and  $m_{zz} = 0.71m_0$  ( $m_0$  is the bare electron mass) along the armchair (ac) and zigzag (zz) directions, respectively.<sup>[5]</sup> LMR has been observed previously in the bulk crystals of bP<sup>[6,7]</sup> yielding only limited progress in its understanding. This is the subject of this work, where an experiment was designed to perform magneto-transport measurements in a 16 nm-thick bP device in the presence of a purely parallel magnetic field that can be rotated in the plane of the bP flake and up to 45 T. A strong classically forbidden LMR was found whose nonmonotonic field dependence closely matches a parabolic behavior. Although LMR has been studied for decades in 3D systems, to our knowledge there is no rigorous theory in 2D anisotropic systems and as such our results call for future theoretical work in this direction.

The geometry of the field-effect transistor (FET) device is shown in **Figure 1a**. Details on device fabrication are provided in Supporting Information (SI). The flake thickness was carefully


Dr. F. Telesio, Dr. M. Carrega, Dr. S. Heun  
NEST  
Istituto Nanoscienze–CNR and Scuola Normale Superiore  
I-56127 Pisa, Italy  
E-mail: francesca.telesio@nano.cnr.it

N. Hemsworth, W. Dickerson, Dr. V. Tayari, Prof. T. Szkopek  
Department of Electrical and Computer Engineering  
McGill University  
Montréal, Québec H3A 2A7, Canada

M. Petrescu, O. Yu, Prof. G. Gervais  
Department of Physics  
McGill University  
Montréal, Québec H3A 2T8, Canada

Dr. D. Graf  
National High Magnetic Field Laboratory  
Tallahassee, FL 32310, USA

Dr. M. Serrano-Ruiz, Dr. M. Caporali, Dr. M. Peruzzini  
Unità di Firenze  
Istituto di Chimica dei Composti Organometallici–CNR  
I-50019 Sesto Fiorentino, Italy

 The ORCID identification number(s) for the author(s) of this article can be found under <https://doi.org/10.1002/pssr.201900347>.

DOI: 10.1002/pssr.201900347

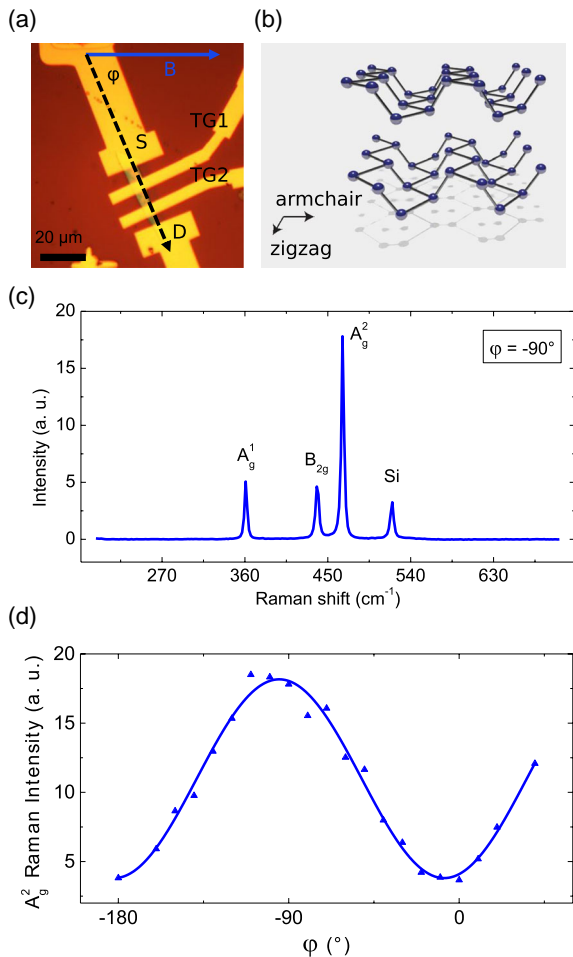


**Figure 1.** a) Optical microscopy image of the device with labeling of source (S) and drain (D) contacts, top gates TG1 and TG2, as well as the definition of the angle  $\varphi$  as the angle between SD and the magnetic field axis. b) The puckered crystal structure of bP with armchair and zigzag directions indicated. c) Raman spectrum of the bP device, with baseline subtracted. The spectrum was acquired at  $\varphi = -90^\circ$ , i.e., with light polarization perpendicular to the device axis. The three bP Raman peaks are labeled, as well as the peak emanating from the Si substrate. d) Polarized Raman measurement.  $A_g^2$  intensity as a function of incoming laser light polarization angle  $\varphi$ . The maximum of  $A_g^2$  is along the armchair axis, the minimum at  $(-5 \pm 2)^\circ$  along zigzag, and therefore the S–D axis of the device is approximately aligned with the zigzag direction of the flake (see Supporting Information for additional details).

determined from atomic force microscopy (AFM) measurements shown in Supporting Information and is  $t = (16 \pm 1)$  nm in the channel region, i.e., around 30 layers, given that the layer-to-layer spacing in bP is 0.524 nm.<sup>[8]</sup> The channel length and average weighted width are  $L = 25.4 \mu\text{m}$  and  $W = 4.4 \mu\text{m}$ , respectively. The transistor includes a conventional back gate and two additional top gates, labeled TG1 and TG2 in Figure 1a, using a combination of  $\text{PO}_x$  and  $\text{Al}_2\text{O}_3$  as oxide dielectrics.<sup>[9]</sup> For the measurements presented here, TG1 is not used. We define  $\varphi$  as the angle between the source–drain (S–D) axis of the device and the in-plane magnetic field used in the experiment (see Figure 1a and 2a). With this convention, at  $\varphi = 0^\circ$ , the magnetic

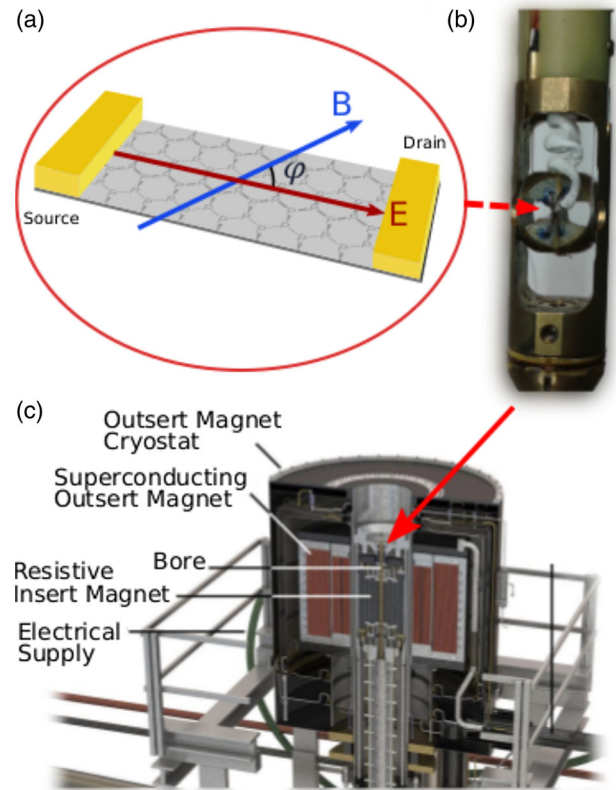


**Figure 2.** a) Schematics of the device with electric field  $E$  and magnetic field  $B$  indicated, as well as crystallographic orientation. The angle  $\varphi$  is defined as the angle between SD and magnetic field axis. b) Photo of the rotator probe as mounted in the cryostat insert. The sample is rotating with the magnetic field in the bP plane. c) Schematics of the hybrid magnet of National High Magnetic Field Laboratory used for high field measurements. The outer, superconducting magnet provides a field in the 0 to 11.4 T range, and together with the resistive insert a field of 45 T can be reached.

field is parallel to the S–D axis and hence to the current ( $B \parallel I$ ), whereas at  $\varphi = \pm 90^\circ$  the magnetic field is perpendicular to the S–D axis and the current ( $B \perp I$ ). For clarity, the same convention has been used in displaying the polarized Raman measurements shown in Figure 1c,d.

The crystal orientation with respect to the S–D axis was determined via polarized Raman spectroscopy. Here, the crystallographic orientation of the bP crystal, shown in Figure 1b, was determined by measuring the Raman peak intensities associated with the in-plane vibrational modes of bP ( $A_g^2$  and  $B_{2g}$ )<sup>[10]</sup> with respect to the linear polarization of the incident laser.<sup>[11,12]</sup> In particular, the maximum of the  $A_g^2$  mode corresponds to the armchair direction.<sup>[10,13,14]</sup> These Raman data are shown in Figure 1d as a function of the polarization angle  $\varphi$ , whereby for  $0^\circ$  the polarization of the incoming laser beam is parallel to the axis of the bP FET channel (dashed line in Figure 1a). From these data, we determine the bP crystal orientation to be such that the zigzag direction is at angle  $\theta = (-5 \pm 3)^\circ$  from the S–D channel axis, as shown in Figure 1d (see also Figure S3, Supporting Information).

During low-temperature magnetotransport measurements, gate voltage dependence revealed an inherent p-type character for bP FET. The device exhibited an intrinsic carrier concentration  $n = 2.2 \times 10^{12} \text{ cm}^{-2}$  and a field-effect mobility  $\mu = 83 \text{ cm}^2 (\text{Vs})^{-1}$  at  $T = 1.64 \text{ K}$  and  $B = 11.4 \text{ T}$ , as provided in the Supporting Information. In all displayed measurements, except when explicitly stated, TG1 and the back gate were kept to ground, whereas TG2 was set to  $-1 \text{ V}$  to increase bP conductance. The device was mounted on a calibrated step-by-step rotator (shown in Figure 2b) that can rotate the sample with the magnetic field axis in the plane of the device. The rotator had an angular resolution within  $0.02^\circ$  which is much less than the systematic errors on  $\varphi$  arising from the crystallographic orientation measurements of bP by Raman spectroscopy. The experiment was performed at low temperatures down to  $300 \text{ mK}$  and up to a  $45 \text{ T}$  magnetic field in the hybrid magnet of the National High Magnetic Field Laboratory in Tallahassee, shown in Figure 2c. The in-plane magnetotransport was investigated by performing several angular sweeps at various magnetic fields, as well as magnetic field sweeps at various angles, to check for data consistency. The normalized MR of the device, defined as  $\Delta R/R = (R(B) - R(0))/R(0)$ , with  $R(0) \equiv R(B = 0) = 173.3 \text{ k}\Omega$ , is shown for various magnetic fields in Figure 3 on the left axis of the graph, whereas the right axis displays the resistance values. Overall, MR is observed to have a strong dependence on the angle  $\varphi$  and varies nonmonotonically with the increasing in-plane magnetic field. Given that a misalignment of  $1^\circ$  at  $45 \text{ T}$  can result in a perpendicular field component of  $0.78 \text{ T}$ , the possible presence of this out-of-plane field was considered. Although the presence of such an out-of-plane component is possible, it cannot itself give rise to the phenomena investigated here. In particular, a potential correction due to weak localization at a high magnetic field is expected to decrease resistance, and therefore it cannot explain the positive LMR observed at the high field.

Upon closer inspection of Figure 3, it becomes apparent that the maxima and minima in MR are not exactly aligned at  $\varphi = 0^\circ$  and  $90^\circ$  (as indicated by the dotted vertical lines in the figure) but instead are slightly shifted to a lower value (as indicated by the arrows). Tracking the angular position of the maximum in MR close to  $-90^\circ$  and the minimum close to  $0^\circ$ , their angular positions are found to be nearly constant at all magnetic fields and given by  $(-94.4 \pm 2.0)^\circ$  and  $(-2.8 \pm 2.0)^\circ$ , respectively.

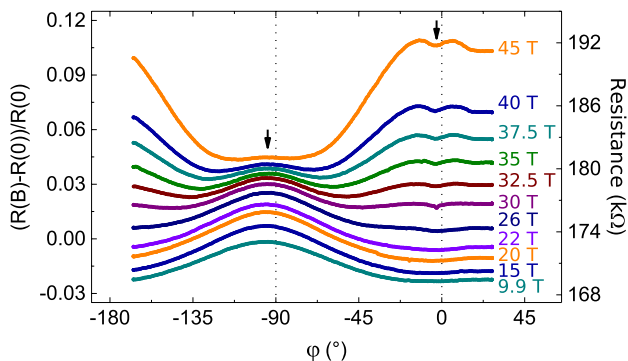


**Figure 3.** Magnetoresistance, defined as  $(R(B) - R(0))/R(0)$ , versus the in-plane angle of rotation  $\varphi$  at various magnetic fields, left axis. The resistance value is shown on the right axis. The data were taken at  $323 \text{ mK}$  temperature.

The  $\pm 2^\circ$  quoted here was estimated from the possible orientation error in mounting the device on the high-magnetic-field sample holder. This significant deviation from the precise values of the device axis suggests that neither the device axis nor the current direction define the relevant coordinate system for the MR. In fact, these angles correspond within error to the orientation of the bP crystal and the directions of zigzag and armchair axes of the bP crystal, indicating that these are the physically relevant directions determining the MR.

Figure 4 displays cross-sections of Figure 3 for the parallel ( $\varphi = 0^\circ$ ) and perpendicular ( $\varphi = -90^\circ$ ) configurations of the magnetic field with respect to the current direction. The LMR ( $\mathbf{B} \parallel \mathbf{I}$ ) is first negative, passes through a minimum at  $\approx 11 \text{ T}$ , and then increases to reach a positive value at  $\approx 26 \text{ T}$ . The LMR is found to take larger value than transverse magnetoresistance (TMR) ( $\mathbf{B} \perp \mathbf{I}$ ) at a crossover field of  $\approx 32.5 \text{ T}$ . Remarkably, the magnetic field dependence of LMR can be well described by a shifted parabola centered at  $B = (11.9 \pm 0.3) \text{ T}$  (red line). In contrast, TMR is nearly constant up to  $11 \text{ T}$  (where LMR reaches its minimum value) and then increases roughly linearly with the increasing in-plane magnetic field.

Resistance measurements taken at fixed angles as a function of magnetic field confirm this trend. These measurements are shown in Figure S4d, Supporting Information. At angles  $\varphi$ , close to  $0^\circ$  and  $-90^\circ$ , the data display a similar crossover, whereas at  $\varphi \approx -180^\circ$  and  $0^\circ$  the data highlight the  $180^\circ$  periodicity of the phenomenon. Finally, upon reversal of the magnetic field, the MR showed no significant dependence on the field direction, see Figure S4e, Supporting Information, except for a slight overall shift that is attributed to a small change in carrier density occurring during a temperature cycling of the device from the base to  $\approx 40 \text{ K}$  temperatures. As the transport measurements were performed in a two-point configuration, the robustness of the observed LMR and TMR against magnetic field polarity ensures that solely in-plane resistivity played a role in the experiment.

To establish the regime of charge transport in the bP flake, we compare the relevant length scales obtained from the experimentally determined carrier density  $n$  and mobility  $\mu$ . We apply a  $2\text{D}$

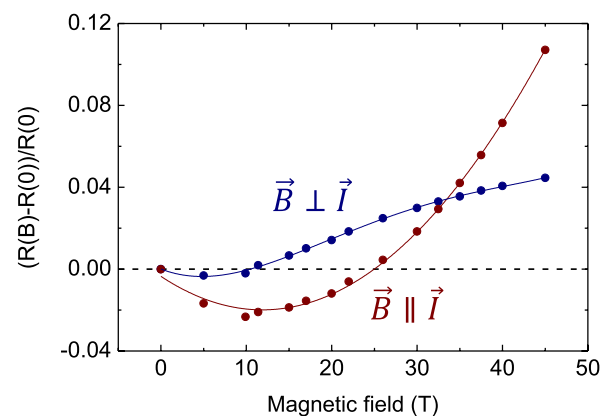


**Figure 4.** Magnetic field dependence of LMR and TMR showing distinct behaviors. It is based on the data shown in Figure 3. The red line is a fit of the LMR ( $\mathbf{B} \parallel \mathbf{I}$ ) data with a shifted parabola centered at  $B = (11.9 \pm 0.3) \text{ T}$ . The blue line is a guide to eye for TMR data ( $\mathbf{B} \perp \mathbf{I}$ ).

Drude model justified here by a self-consistent Schrödinger–Poisson calculation, showing that the charge density in bP flakes on SiO<sub>2</sub> is concentrated within a surface accumulation layer with a mean thickness,  $\langle z \rangle \approx 3$  nm.<sup>[15]</sup> Within the effective mass approximation, hole dispersion is given by  $E = \delta + \hbar^2 k_{zz}^2 / 2m_{zz} + \hbar^2 k_{ac}^2 / 2m_{ac}$ ,<sup>[16]</sup> with  $\delta$  as the band gap, quantifying the anisotropy in charge carrier motion along zigzag and armchair directions.

The Fermi wavevector is itself anisotropic, with the relevant Fermi wavevector being  $k_{F,zz}$  for charge carriers moving in the zigzag direction with current flow in the bP flake. The wavevector is  $k_{F,zz} = (m_{zz}/m_{ac})^{1/4} (2\pi n)^{1/2} = 0.59$  nm<sup>-1</sup>, which corresponds to a Fermi wavelength  $\lambda_{F,zz} = 2\pi/k_{F,zz} = 10.6$  nm. The Fermi wavelength is larger than the mean thickness  $\langle z \rangle$  of the accumulation layer and smaller than the flake thickness  $t$ . The Fermi velocity  $v_{F,zz}$  along the zigzag axis is  $v_{F,zz} = \hbar k_{F,zz} / m_{zz} = 9.7 \times 10^4$  ms<sup>-1</sup>. The elastic scattering time  $\tau_{zz} = m_{zz} \mu / e = 3.3 \times 10^{-14}$  s and the elastic mean free path  $\ell_{e,zz} = v_{F,zz} \tau_{zz} = 3.2$  nm,<sup>[17]</sup> where mobility  $\mu = \mu_{zz}$  was measured for current flow along the zigzag axis. The mean free path  $\ell_{e,zz}$  is similar to the thickness of the accumulation layer  $\langle z \rangle$ .

The Ioffe–Regel criterion for localization<sup>[18,19]</sup> can be used to ascertain the regime of charge transport. We find  $k_{F,zz} \ell_{e,zz} = 1.9$ , indicating that transport within our bP device is diffusive, albeit close to the crossover from diffusive to localized transport ( $k_F \ell_e = 1$ ). We can compare the length scales of charge carrier transport with the magnetic length  $\ell_B = \sqrt{\hbar/eB}$ , which decreases from 11.4 nm at  $B = 5$  T to 3.8 nm at  $B = 45$  T. Only at the highest fields used in our experiments does the magnetic length approach the thickness of the accumulation layer.

A negative MR in the strongly localized regime has been observed before and has been ascribed to the orbital MR due to quantum interference among random paths in the hopping process.<sup>[20,21]</sup> In particular, it was reported that an anisotropy in the MR is indicative of this magneto-orbital mechanism and that this orbital MR is always negative.<sup>[21]</sup> Later work suggested that inclusion of spin–orbit scattering in the theory can lead to a positive MR.<sup>[22,23]</sup> Such positive MR in the strongly localized regime has been observed in many disordered materials.<sup>[24]</sup> However, this reasoning is unlikely to be applicable here given that spin–orbit coupling in bP is so weak.<sup>[5,25]</sup> In addition, the in-plane anisotropy of the  $g$  factor of bP is also negligible ( $g_{ac} \approx g_{zz}$ )<sup>[26,27]</sup> and close to the bare electron value,  $g = 2$ , indicative of negligible exchange enhancement.<sup>[26]</sup>

Nonclassical LMR has been observed in a variety of systems ranging from 3D metals, topological materials, to semiconductors (see studies by Goswami et al.<sup>[2]</sup> for a recent discussion). In the 1960s, this phenomenon attracted interest in the context of metals with nontrivial FS<sup>[28]</sup> and subsequently in semiconductors with nonparabolic bands.<sup>[29]</sup> More recently, it has been discussed for massless Dirac and Weyl fermionic systems.<sup>[1,2,30]</sup> In 2010, Pal and Maslov<sup>[4]</sup> derived the necessary and sufficient conditions for the occurrence of LMR within the context of FS morphology of a 3D electronic system; while they have shown that an anisotropic FS is a prerequisite, not all types of anisotropies will give rise to the effect. They specified that an angular anisotropy of the FS along the magnetic field direction is a sufficient condition in three dimensions. Our case, for which the

electronic system is defined by a 2D hole gas confined at the bP/SiO<sub>2</sub> interface, provides an interesting example of anisotropic FS as the bP FS is elliptical and its effective masses in the armchair and zigzag directions differ by a factor of  $\approx 7$ .

While Pal and Maslov studied the conditions for LMR to occur on generic grounds for a 3D system, a quantitative theoretical description for LMR in 2D systems with anisotropic FS is still lacking. Moreover, Goswami et al.<sup>[2]</sup> state that for a 3D metal the existence of a finite LMR is purely a quantum mechanical effect and a direct consequence of the axial anomaly. Furthermore, they showed that in the presence of both neutral and ionic impurities, the LMR becomes first negative for low fields, and then positive for high fields after passing through a minimum, which is reminiscent of what is observed in the LMR data shown in Figure 4. We caution, however, that their theory was developed for the quantum limit where  $\omega_c \tau \gg 1$ , with  $\omega_c$  the cyclotron frequency and  $\tau$  the elastic scattering time. Nevertheless, Goswami et al.<sup>[2]</sup> underline the good agreement of their results with calculations of Spivak and coworkers in the semiclassical<sup>[1]</sup> and diffusive regime,<sup>[3]</sup> both valid for  $\omega_c \tau \ll 1$ . These recent theoretical advances suggest that a similar framework should be developed in 2D systems, especially given the present interest in 2D atomic crystals of all kinds. For instance, it is known that applying a purely parallel magnetic field on a 2D electron gas (2DEG) can lead to a magneto-orbital coupling sufficient to generate a substantial MR, as proposed theoretically by Das Sarma and Hwang,<sup>[31]</sup> and found experimentally in GaAs 2DEGs with finite widths.<sup>[32]</sup> The bP being a simple system to test the effects of FS anisotropy, it is in our view likely that FS anisotropy can lead to MR modulation found in this work, even though no quantitative theory in 2D exists at the moment.

The classically forbidden LMR has been studied in different material systems for decades, and only recently the conditions under which it can be observed were explored theoretically in three dimensions. One clear route toward an LMR in 3D involves an anisotropic FS, and in its simplest expression an anisotropic FS in 2D can be thought out of an ellipse. Our work on bP at a high magnetic field provides an important example for the appearance of LMR in a 2D anisotropic system, and such observations of LMR for all fields inspected are confirmed. This LMR was discovered to be strongly anisotropic, nonmonotonic, positive beyond  $\approx 26$  T, and dominant in strength beyond  $\approx 30$  T. Even though the magnetic length at the highest magnetic field used here (45 T) is more than one order of magnitude larger than the phosphorus bond length, this LMR work demonstrates once more the potential generated by high magnetic fields in the understanding of band structure effects on charge transport in atomic crystals. Our experimental data strongly suggest that anisotropy most likely plays an important role in the appearance of LMR, thereby calling for theoretical descriptions of magneto-transport properties in the presence of anisotropic FS to be developed.

## Supporting Information

Supporting Information is available from the Wiley Online Library or from the author.

## Acknowledgements

The authors are grateful to Danil Bukhvalov, Alina Mreńca–Kolasnińska, and Bartłomiej Szafran for helpful discussions. This work was funded by NSERC (Canada), CIFAR, FRQNT (Québec), and the CRC program (T.S. and G.G.). A portion of this work was performed at the National High Magnetic Field Laboratory which was supported by NSF Cooperative Agreement No. DMR-1157490, and the State of Florida. F.T., M. S.-R., M. Caporali, M.P., and S.H. thank the European Research Council for funding the project PHOSFUN *Phosphorene functionalization: a new platform for advanced multifunctional materials* (Grant Agreement No. 670173) through an ERC Advanced Grant to M.P. F.T. acknowledges financial support by CNR Nano through the SEED project SURPHOS. S.H. acknowledges support from Scuola Normale Superiore, Project No. SNS16 B HEUN-004155. M. Carrega acknowledges support from the bilateral project CNR/Royal Society number IES/R3/170252.

## Conflict of Interest

The authors declare no conflict of interest.

## Keywords

anisotropy, black phosphorus, longitudinal magnetoresistance

Received: June 17, 2019

Revised: July 23, 2019

Published online: September 4, 2019

- 
- [1] D. T. Son, B. Z. Spivak, *Phys. Rev. B* **2013**, *88*, 104412.  
 [2] P. Goswami, J. H. Pixley, S. Das Sarma, *Phys. Rev. B* **2015**, *92*, 075205.  
 [3] A. Andreev, B. Z. Spivak, *Phys. Rev. Lett.* **2018**, *120*, 026601.  
 [4] H. K. Pal, D. L. Maslov, *Phys. Rev. B* **2010**, *81*, 214438.  
 [5] J. Qiao, X. Kong, Z. X. Hu, F. Yang, W. Ji, *Nat. Commun.* **2014**, *5*, 4475.  
 [6] T. Strutz, N. Miura, Y. Akahama, *Physica B* **1994**, *194–196*, 1185.  
 [7] Z. Hou, B. Yang, Y. Wang, B. Ding, X. Zhang, Y. Yao, E. Liu, X. Xi, G. Wu, Z. Zeng, Z. Liu, W. Wang, *Sci. Rep.* **2016**, *6*, 23807.  
 [8] A. Morita, *Appl. Phys. A: Solids Surf.* **1986**, *39*, 227.  
 [9] W. Dickerson, V. Tayari, I. Fakhri, A. Korinek, M. Caporali, M. Serrano-Ruiz, M. Peruzzini, S. Heun, G. A. Botton, T. Szkopek, *Appl. Phys. Lett.* **2018**, *112*, 173101.  
 [10] S. Sugai, I. Shirovani, *Solid State Commun.* **1985**, *53*, 753.  
 [11] X. Chen, X. Lu, B. Deng, O. Sinai, Y. Shao, C. Li, S. Yuan, V. Tran, K. Watanabe, T. Taniguchi, D. Naveh, L. Yang, F. Xia, *Nat. Commun.* **2017**, *8*, 1672.  
 [12] X. Wang, A. M. Jones, K. L. Seyler, V. Tran, Y. Jia, H. Zhao, H. Wang, L. Yang, X. Xu, F. Xia, *Nat. Nanotechnol.* **2015**, *10*, 517.  
 [13] J. Kim, J. U. Lee, J. Lee, H. J. Park, Z. Lee, C. Lee, H. Cheong, *Nanoscale* **2015**, *7*, 18708.  
 [14] A. L. Phaneuf-L'Heureux, A. Favron, J. F. Germain, P. Lavoie, P. Desjardins, R. Leonelli, R. Martel, S. Francoeur, *Nano Lett.* **2016**, *16*, 7761.  
 [15] V. Tayari, N. Hemsworth, I. Fakhri, A. Favron, E. Gaufres, G. Gervais, R. Martel, T. Szkopek, *Nat. Commun.* **2015**, *6*, 7702.  
 [16] A. Chaves, W. Ji, J. Maassen, T. Dumitrica, T. Low, in *2D Materials. Properties and Devices*, Cambridge University Press, Cambridge **2017**, pp. 381–412.  
 [17] T. Ando, A. B. Fowler, F. Stern, *Rev. Mod. Phys.* **1982**, *54*, 437.  
 [18] M. Gurvitch, *Phys. Rev. B* **1981**, *24*, 7404.  
 [19] P. A. Lee, T. V. Ramakrishnan, *Rev. Mod. Phys.* **1985**, *57*, 287.  
 [20] U. Sivan, O. Entin-Wohlman, Y. Imry, *Phys. Rev. Lett.* **1988**, *60*, 1566.  
 [21] O. Faran, Z. Ovadyahu, *Phys. Rev. B* **1988**, *38*, 5457.  
 [22] J. L. Pichard, M. Sanquer, K. Slevin, P. Debray, *Phys. Rev. Lett.* **1990**, *65*, 1812.  
 [23] P. Hernandez, M. Sanquer, *Phys. Rev. Lett.* **1992**, *68*, 1402.  
 [24] W. Jiang, J. L. Peng, J. J. Hamilton, R. L. Greene, *Phys. Rev. B* **1994**, *49*, 690.  
 [25] Z. S. Popović, J. M. Kurdestany, S. Satpathy, *Phys. Rev. B* **2015**, *92*, 035135.  
 [26] L. Li, F. Yang, G. J. Ye, Z. Zhang, Z. Zhu, W. Lou, X. Zhou, L. Li, K. Watanabe, T. Taniguchi, K. Chang, Y. Wang, X. H. Chen, Y. Zhang, *Nat. Nanotechnol.* **2016**, *11*, 593.  
 [27] X. Zhou, W. K. Lou, D. Zhang, F. Cheng, G. Zhou, K. Chang, *Phys. Rev. B* **2017**, *95*, 045408.  
 [28] A. B. Pippard, *Proc. R. Soc. London, Ser. A* **1964**, *282*, 464.  
 [29] U. P. Phadke, S. Sharma, *J. Phys. Chem. Solids* **1975**, *36*, 1.  
 [30] A. Sekine, D. Culcer, A. H. MacDonald, *Phys. Rev. B* **2017**, *96*, 235134.  
 [31] S. Das Sarma, E. H. Hwang, *Phys. Rev. Lett.* **2000**, *84*, 5596.  
 [32] X. Zhou, B. A. Piot, M. Bonin, L. W. Engel, S. Das Sarma, G. Gervais, L. N. Pfeiffer, K. W. West, *Phys. Rev. Lett.* **2010**, *104*, 216801.